33RD CONGRESS
OF THE INTERNATIONAL COUNCIL
OF THE AERONAUTICAL SCIENCES
STOCKHOLM, SWEDEN, 4-9 SEPTEMBER, 2022

ICAS 2022 SWEDEN

THE USE OF COMPUTATIONAL FLUID DYNAMICS METHODS IN THE PRELIMINARY DESIGN OF A NEW GENERATION LIGHT COMBAT AIRPLANE

Łukasz Kiszkowiak[1], Aleksander Olejnik[1], Adam Dziubiński[2],

[1] Military University of Technology, Faculty of Mechatronics, Armament and Aerospace,
2 gen. Sylwestra Kaliskiego Str., 00-908, Warsaw,
lukasz.kiszkowiak@wat.edu.pl, aleksander.olejnik@wat.edu.pl, tel. +48261837374
[2] Łukasiewicz Research Network – Institute of Aviation, Aerodynamics Department, Al. Krakowska 110/114,
02-256, Warsaw, adam.dziubinski@lukasiewicz.ilot.gov.pl, tel. +48221883743

Abstract

The change in the nature of threats and armed conflicts forced a change in the way they were conducted and the need to develop a new types of weapons. In the following paper the basic design assumptions of a new generation light combat airplane have been presented. The technical data of the developed versions of the airplane were shown. What is more, the results of the aerodynamic characteristics identification process of the newly designed object were presented. In past decades a massive improvement of computational fluid dynamics methods and the rapid increase of computational resources made it possible to simulate a lot of phenomena appearing during the flow of fluid around an object. Aerodynamic analysis was performed using specialized software based on solving partial differential equations using the Finite Volumes Method. The aerodynamic analysis results were presented in the form of diagrams showing aerodynamic force and moment components as a function of the angle of attack. In addition, qualitative results of the flow around the plane have been presented. Presented results prove that adopted method is sufficient for solving this type of problems.

Keywords: conceptual aircraft design**,** Computational Fluid Dynamics, aerodynamic layout, Finite Volumes Method, airplane

1. Introduction

The main purpose of this work was to obtain, using Computational Fluid Dynamics methods, a reliable information on aerodynamic properties of newly designed airplane OSA-3 (in English: WASP-3) shown in Figure 1. The design process of an airplane that meets the imposed criteria in the set of acceptable solutions controlled by the constraints resulting from the planned missions is a complex process. It is inevitable in the design process, that the assumptions made at the beginning do not meet the expectations in terms of the “perfection” of airplane's aerodynamic layout. Such a phenomenon forces to change the shape of airframe and assume better value of its parameters, and proceeding to the next iteration of the design process [1 – 3]. In recent years the development of new, more reliable tools for "multiphysics" calculations allowed the designers to address more problems at the very beginning (or at early stages) of the design process [4, 5]. The authors decided to use an ANSYS Fluent v.15 software [6] based on solving partial differential equations using the finite volumes method [7, 8]. Various science papers [9 – 12] show the possibilities for using numerical methods to possess overall information regarding the aerodynamic characteristics of aircraft or its parts. Worth of mentioning is also, that such a method can be used in further design, starting from the influence of deflected control surfaces, influence of the propeller, and even the cooling systems of the engine and cabin could be tested [13 – 15]. Also the armament drop safety can be tested [16 – 18] in order to avoid contact with the fuselage or other part of the aircraft.

The OSA-3 is a light two-seat combat airplane that will be made of high-strength composite materials as well as duralumin and steel. This version of aircraft is powered by a turboprop engine in a pusher configuration. The cabin has been designed in a tandem configuration. The weapon systems operator seat is at the front, while pilot seat is at the rear of cabin. The cabin and fuel tank were partially armored. The wings were equipped with fixed slots and Fowler flaps. The armament of the aircraft is a machine gun and air-to-ground missiles.

Figure 1 – The visualization of new generation light combat airplane OSA-3 (in English: WASP-3).

The main features of OSA-3 aircraft are:

- short take-off and landing capabilities;
- high performance – high cruising speed and rate of climb;
- high maneuverability;
- operation from unprepared runways, during day and night conditions, from grass, snow and water;
- simplified maintenance, even in the field;
- low empty weight – approx. 350 kg.

Specifications, general characteristics and performance of the combat version of the OSA-3 aircraft:

- wingspan: 8 m
- length: 7.2 m
- wing area: 10 m^2
- wing aspect ratio: 6.4
- maximum take-off weight: 900 kg
- empty weight: 350 kg
- maximum speed: 350 km/h
- stall speed: 70 km/h
- climb speed: 15 m/s
- range: 700 km
- take-off/landing distance: < 100 m

In order to improve the training process of pilots and to increase the number of institutions interested in purchasing the OSA-3 airplane, an unarmed – civil version is also being developed. This version will be propelled by a Rotax piston engine. The use of a piston engine will significantly reduce operating costs. What is more, the lack of additional armament will reduce the overall weight of the structure. That is why, this version of aircraft will have similar performance to the combat version.

Specifications, general characteristics and performance of the civil version of the OSA-3 aircraft:

- wingspan: 8 m
- length: 7.2 m
- wing area: 10 m^2
- wing aspect ratio: 6.4
- maximum take-off weight: 600 kg
- empty weight: 350 kg
- maximum speed: 250 km/h
- stall speed: 60 km/h
- climb speed: 6 m/s
- range: 700 km
- take-off/landing distance: < 150 m

2. Computational model

The use of Computational Fluid Dynamics methods at the stage of designing the airplane aerodynamic layout significantly accelerates the implementation of the project at particular stages of the design spiral. Moreover, it speeds up the variation process and facilitates the evaluation of further project development. The design process of an airplane aerodynamic layout at the stage of conceptual design and preliminary design must be preceded by a stage of assumptions and determination of the most important criteria, the fulfillment of which is a necessary condition in the subsequent stages of aircraft design [19 – 21]. In following paper the impact of fuselage size and shape, engine nacelles and tail modifications (Figure 2) on the aerodynamic characteristics of the aircraft has been described. Bearing this fact in mind, this article's novelty is based mainly on the use of CFD methods to analyze the aerodynamic properties of a newly design airplane with unconventional aerodynamic layout.

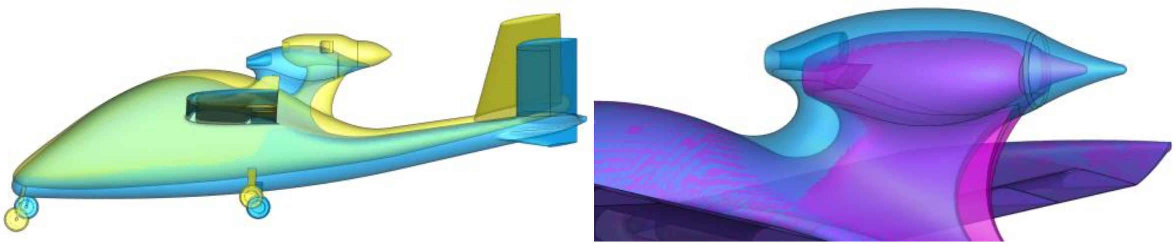

Figure 2 – Comparison of two side views of fuselage modification and two versions of engine nacelle analysed in following paper.

Usually the designer's first approach to fuselage design is to fit all necessary equipment and crew inside, and assume that the internal structure will fit to allow the loads appearing during flight to be transferred to and from the aerodynamic surfaces and overall static and dynamic stability of airframe will be achieved [1, 19]. After the CFD calculation the aerodynamic forces distribution on this first iteration (Figure 3) is known, so the first approach of the structural design (usually with FEM method) can start, and there the critical parts of the fuselage, where the internal forces extend their limits, are changed. After this, those changes have to be validated by the next iteration of the CFD process, and this design loop repeats converging rather fast into the final shape of the fuselage.

Comparing the shapes of the fuselage on Figure 2, or better using Figure 3 and 4 one can find, that the cabin area was shortened, the critical shape of the translation between the cockpit and the tail - has been widened and extended sideways to provide the stiffness against side forces and bending moments. What is more, the tail surfaces have changed and anti - spin surfaces at the bottom of the tail appeared, so overall design allows the airframe to better fit above explained purposes while being safer, better provided against spin in "low and slow" flight conditions and more safe if anything happens.

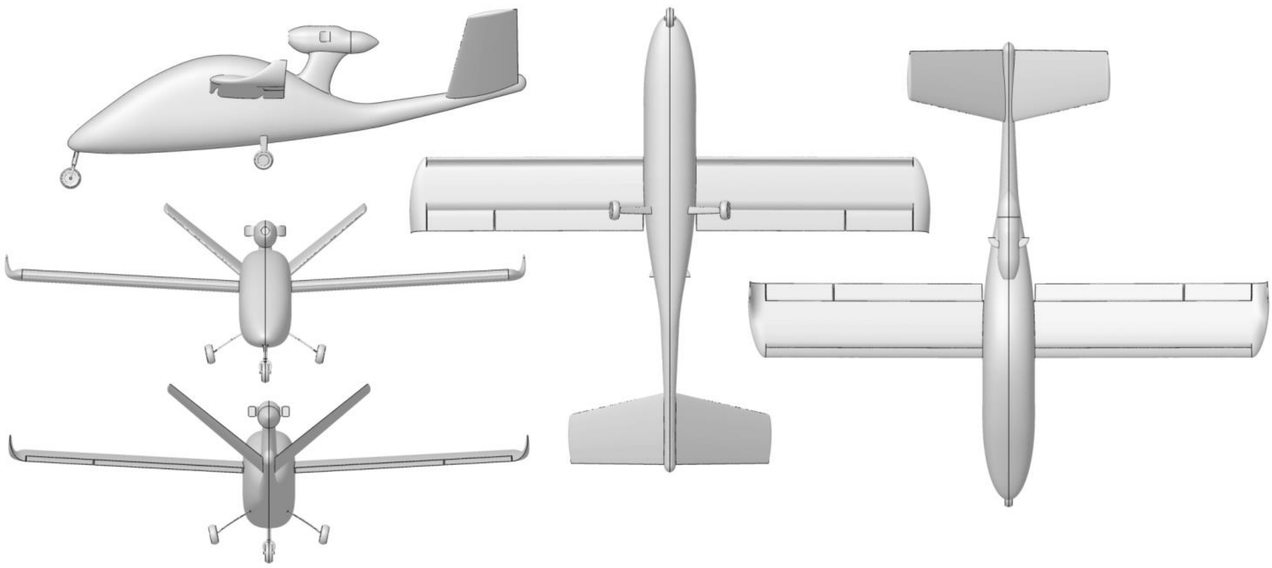

Figure 3 – Views of the preliminary design with initial shape of the fuselage.

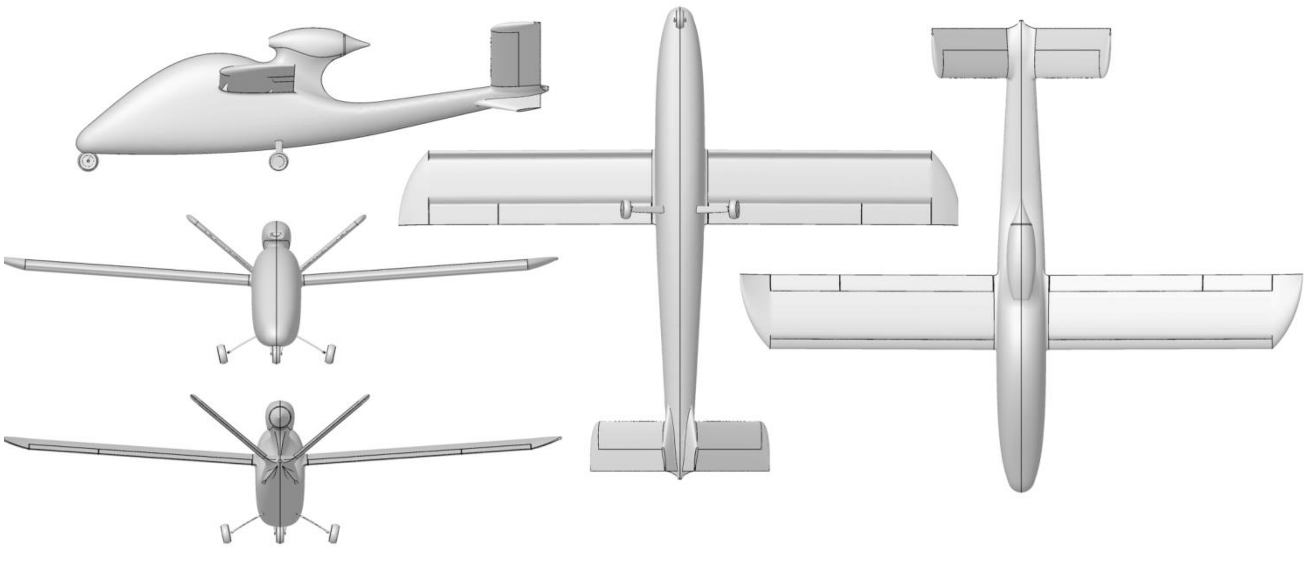

Figure 4 – Views of the final design shape of the fuselage.

3. CFD model: mesh and boundary conditions

A numerical model of each aircraft configuration (and a few in between) has been developed using Computer Aided Design and ANSYS ICEM v.15 software [22]. The model was intended to be analyzed with the ANSYS Fluent v.15 software [6], one of the most recognized industrial standard codes. The shape of aircraft was surrounded by the computational domain, shown in Figure 5. The computational domain was created with assumption that there will be a symmetry of flow along with geometrical symmetry of the airframe. All sideslip calculations demanding the other half of the domain, are then easy to obtain using symmetry and replacing the symmetry condition with an internal wall - which is "invisible" to the flow.

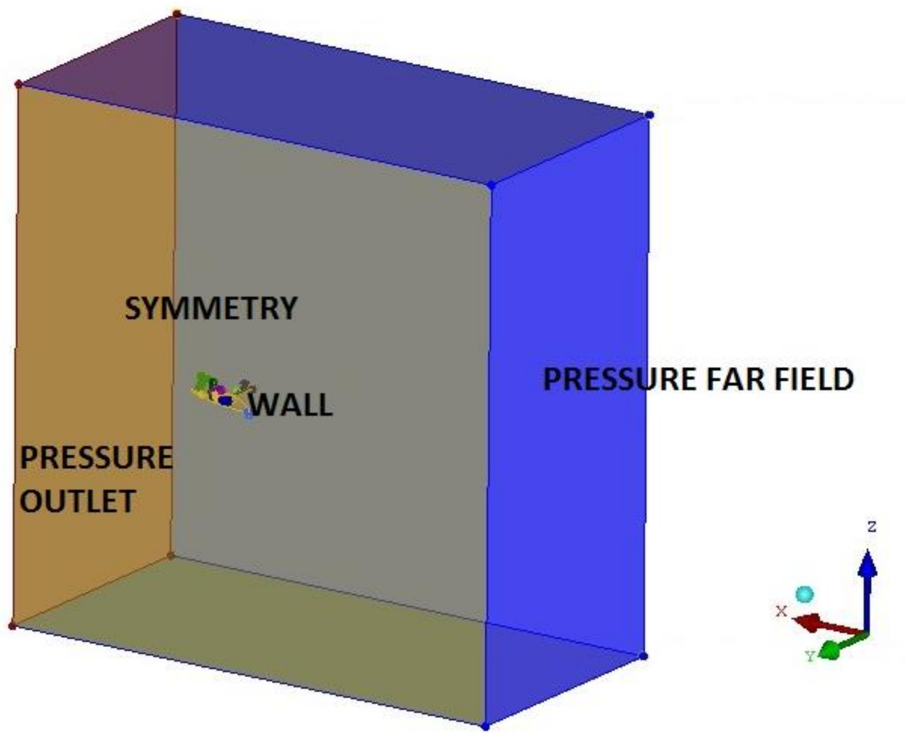

Figure 5 – The computational domain.

The computational domain is much bigger than the plane itself. That size of the computational domain provides better conditions for the calculation to converge, the fluid has a lot more volume for turbulence energy to dissipate, and overall stability of the solution is better, even after a stall (flow detachment on the upper surface of the wings).

Around the computational domain a pressure far field condition allows to set a proper angle of attack, and all the disturbances caused by the airframe are led out of the domain through the pressure outlet condition. This way even if the source of energy or momentum appears in the domain (i.e. working propeller), the energy does not accumulate, instead it is led out "safer way" than it would be if the whole back was covered by the pressure far field condition. Last but not least, all the airframe surfaces are defined as no slip walls.

All the walls are equipped with few layers of prismatic elements forming so called "boundary layer mesh inflation", a special region to catch all the phenomena within the boundary layer: its turbulization and eventually - flow detachment. It is very necessary to have such in any case, but this specific airplane has a STOL (Short TakeOff and Landing) characteristics and is equipped with slats on wings leading edges and slotted flaps and flaperons on its trailing edges. Therefore a proper resolving of the boundary layer on those wings is crucial. All the other elements of mesh are tetrahedral, and those allow to easy generate an unstructured mesh around all complicated geometries. The use of structured mesh is no longer as necessary in this flight regime, because the computational methods improved so much, that the results are comparable and the meshing effort is a lot lower. The calculation was done using the robust Spalart-Allmaras turbulence model with Y+ parameter of the mesh within the 30-200 range. This model is adopted as a standard in the analysis of external flows, especially in the range of Reynolds numbers used in aviation [7, 8].

Figure 6 shows the density of the computational mesh generated on the basis of geometric models of the OSA-3 aircraft. Noteworthy is the higher mesh density in areas of the expected high variability of the flow parameters being determined. Such areas include, but are not limited to: leading edges and trailing edges of the wing and control surfaces, wing-fuselage connection area and areas of significant surface curvature change.

For performing numerical aerodynamic analyzes in symmetrical flow around an object, the following assumptions were made:

- symmetry of the flow field;
- symmetry of geometry;
- the flow is stationary and stable, i.e. there is neither Karman vortex path behind the airframe nor any other non-stationary structure in the flow;
- flight conditions correspond to the zero altitude (at the sea level) according to the reference atmosphere: pressure p=101325 Pa, temperature T=288.15 K, and air density ρ=1.225 kg/m^3.

The position of the pole of the aerodynamic moment was on the plane of symmetry of the aircraft at the point corresponding to the projection of the ¼ SCA point on this plane.

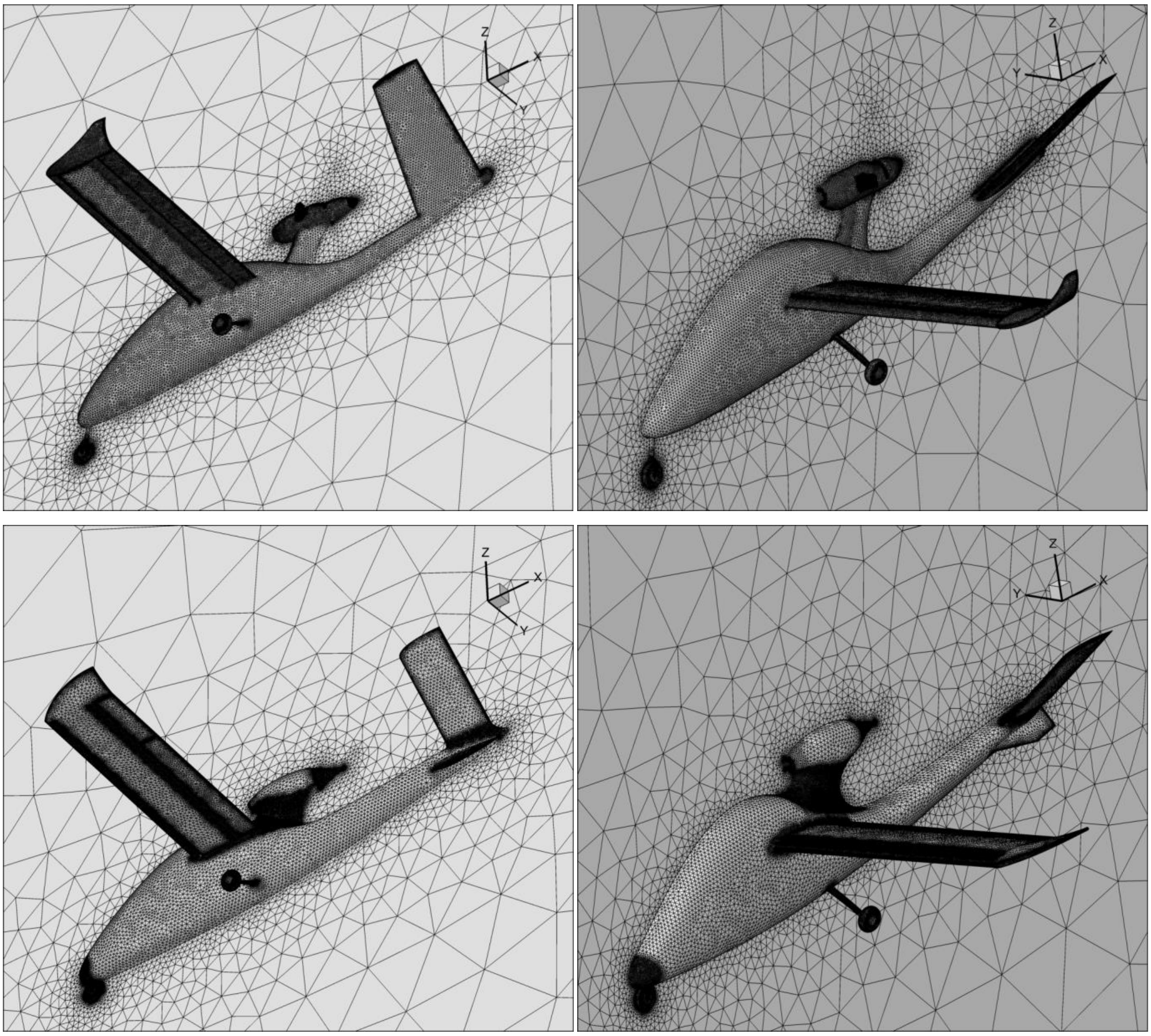

a) b)

Figure 6 – The computational mesh density around the preliminary design (a) and final design (b) of the OSA-3 aircraft.

4. Results and Discussion

During aerodynamic analysis, the right-handed Cartesian coordinate systems were used [7, 8]. Local (airframe) coordinate system is defined as follows: its center appears in a center of mass of the aircraft. The Oxz datum plane is a plane of aircraft's geometrical, inertial and aerodynamical symmetry. Ox axis belongs to the airframe's symmetry plane, is a main inertial axis and is directed forward. Oy axis is perpendicular to the symmetry plane and is directed right from symmetry plane, along with right wing. Oz axis also belongs to the symmetry plane, is perpendicular to both others and is directed down.

An aerodynamic coordinate system was defined in a following way:

- center in the same point "O" as the local coordinate system;
- Oxa axis is directed along the velocity vector;
- Oza axis belongs to the symmetry plane of the aircraft;
- Oya is perpendicular to both axes, and is directed as for the right-handed coordinate system, to the right wing.

Moreover angle of attack α was defined as an angle between the velocity vector V projected on the symmetry plane of the aircraft and its longitudinal Ox axis. Figure 7 shows the aircraft size, coordinate systems position, positive directions of forces and angle of attack α.

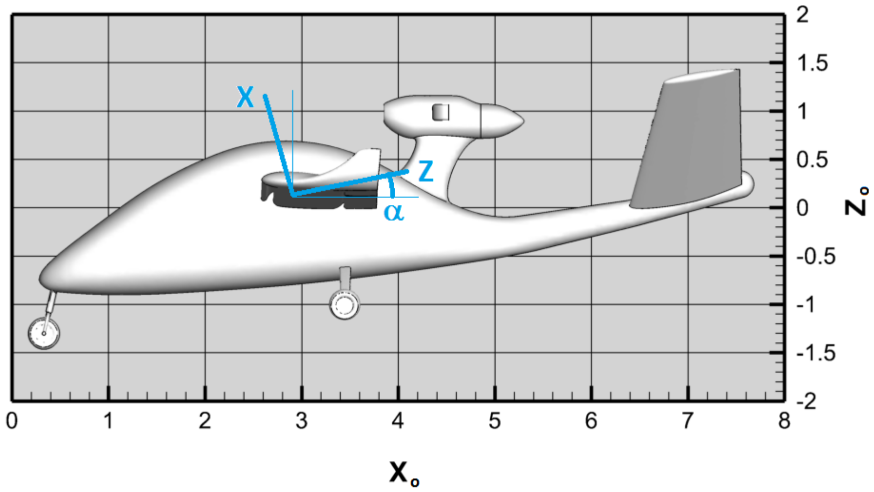

Figure 7 – The aircraft size, coordinate systems position, positive directions of forces and angle of attack [dimension in meters].

The following formulas [7, 8] were used to find the aerodynamic coefficients:

- drag force coefficient

$$C_D = \frac{2 \cdot F_D}{\rho_\infty \cdot v_\infty^2 \cdot S} \tag{1}$$

- lift force coefficient

$$C_L = \frac{2 \cdot F_L}{\rho_\infty \cdot v_\infty^2 \cdot S} \tag{2}$$

- pitching moment coefficient

$$C_m = \frac{2 \cdot M}{\rho_\infty \cdot v_\infty^2 \cdot S \cdot MAC} \tag{3}$$

where:
F_D – drag force [N];
F_L – lift force [N];
M – pitching moment [Nm];
ρ_∞ – air density [kg/m^3];
v_∞ – undisturbed flow velocity [m/s];
S – lifting surface [m^2];
MAC – mean aerodynamic chord [m].

Natural way of understanding of calculation results are the results for the whole airframe as in the wind tunnel. But an unique ability of the CFD methods over the experimental ones is a possibility to obtain the loads on specific parts of airframe as wing, flap or slat, separately. It is easier to obtain the forces and moments on their connections to the structure that way. Therefore, due to the adopted method for presenting the results of the calculations, the surfaces of the aircraft were divided into appropriate zones, which are shown in Figure 8.

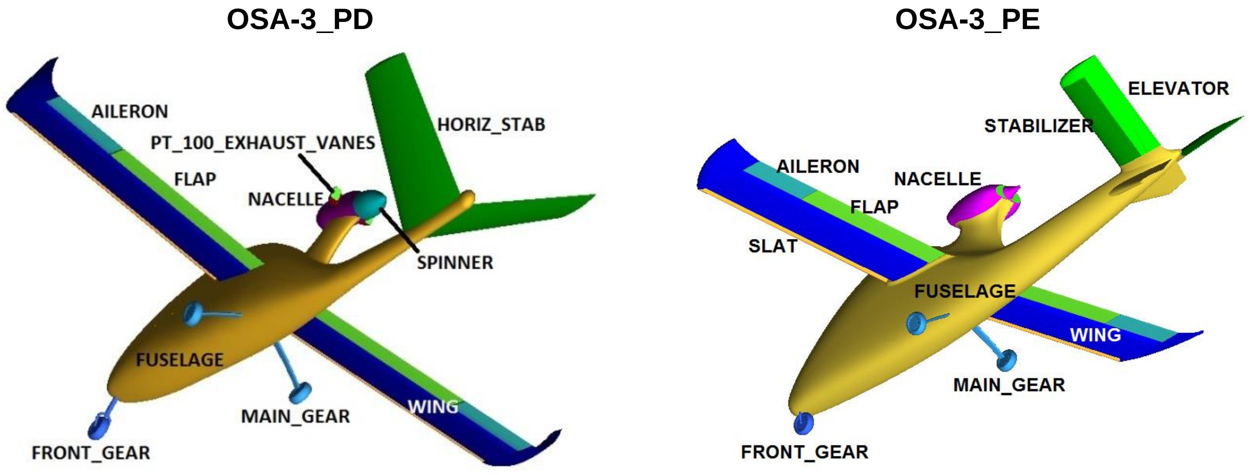

Figure 8 – Division of the aircraft airframe surfaces into appropriate computational zones.

The named zones corresponding to the airframe elements are slightly different along the design, but still allow to compare the aerodynamic interference and load share of the corresponding parts (Figures 9 -11). In the case of the drag coefficient (Figure 9), the main sources of the drag are the wings and fuselage. The share of wing, fuselage and tail section in the total value of the drag force coefficient increases with the increase in the absolute value of the angle of attack. The share of the wing in the value of the lift coefficient (Figure 10) is large (almost 70%), while the share of the fuselage accounts for approx. 15% of the total value of the lift coefficient. These proportions do not change radically with the change of the angle of attack. On the characteristics of the pitching moment coefficient (Figure 11) it can be notice the unstable influence of the fuselage and a much greater stable influence of the tail section.

Moreover, the obtained results prove that the fuselage has bigger drag at the extreme angle of attack (Figure 9), but its pitching moment characteristics, especially at stall, prove better stability in pitch over the preliminary design version (Figure 11). The lift provided by the fuselage also improved a little (Figure 10).

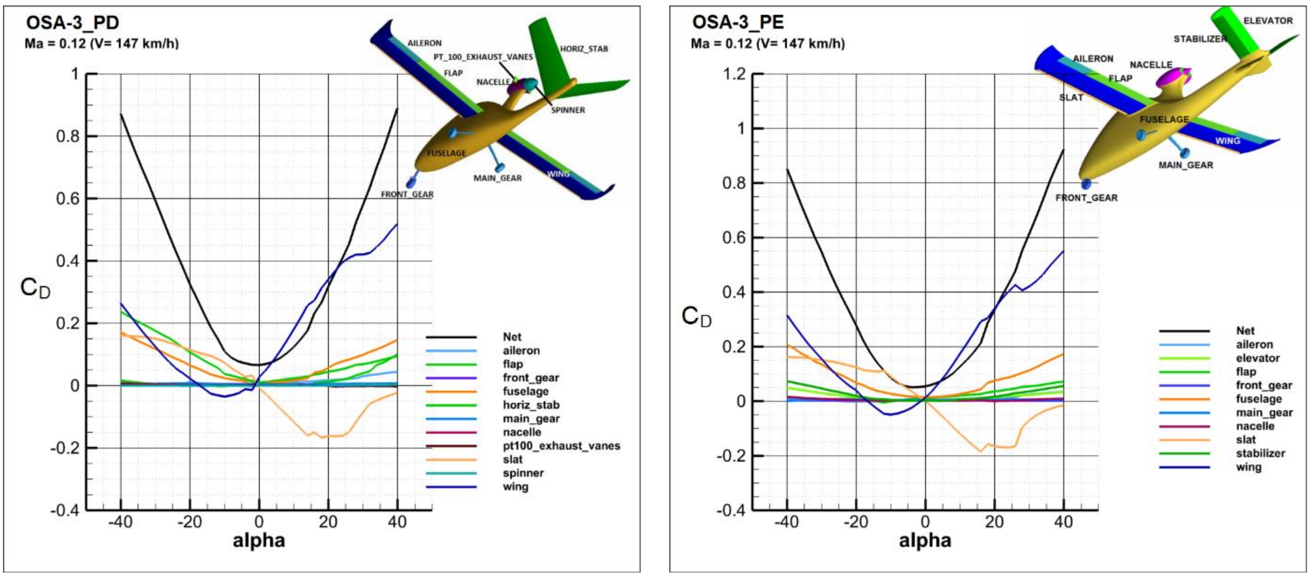

Figure 9 – Comparison between drag coefficient distributon for the preliminary design (left) and final design (right).

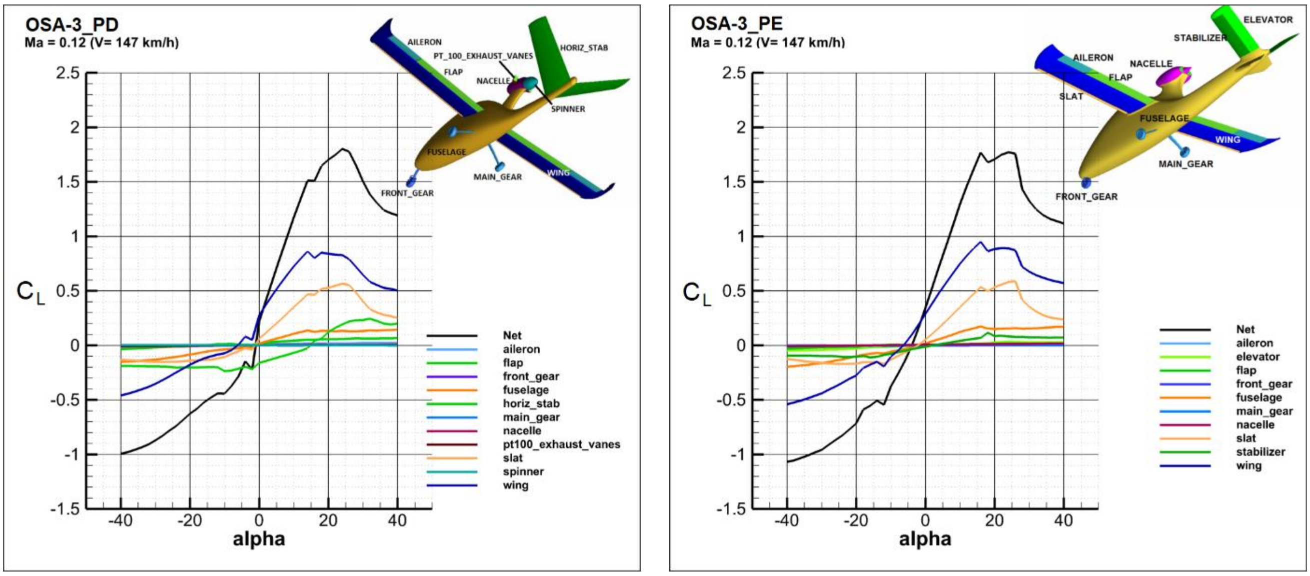

Figure 10 – Comparison between lift coefficient distributon for the preliminary design (left) and final design (right).

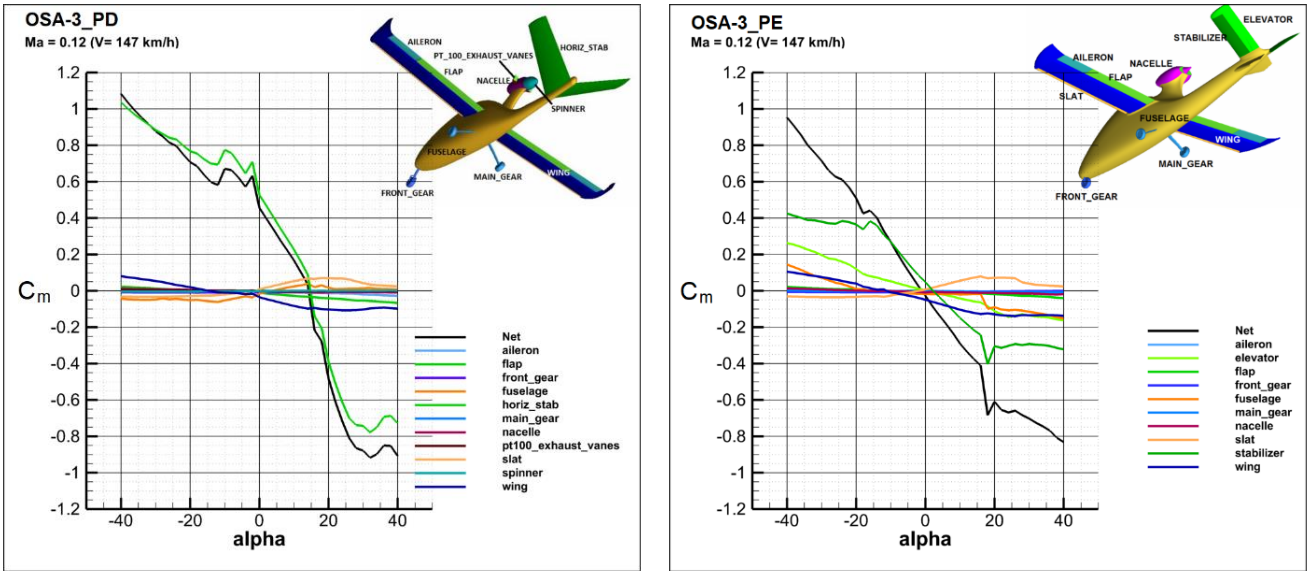

Figure 11 – Comparison between pitching moment coefficient distributon for the preliminary design (left) and final design (right).

The qualitative results are illustrated with maps allowing to obtain the information about both pressure distribution and the flow detachment using pathlines (Figure 12) and the maps of reverse flow (Figure 13) for stall visualization. The areas of separation, i.e. the areas of reverse flow, were depicted using the friction coefficient component along the aircraft axis. The coloring areas have been trimmed so as to color only the surfaces where the flow is in the opposite direction to the undisturbed flow. Figure 12 shows a comparison of pressure distribution along with the pathlines flow visualization for three aircraft versions at the same angle of attack α=14°:

- OSA-3_PD – initial aircraft version,
- OSA-3_TP – final aircraft version with turboprop engine,
- OSA-3_PE – final aircraft version with piston engine (different engine nacelle case and mast on which the engine is mounted).

In addition, Figure 13 presents evolution of stall visualized by the areas of reverse flow along with the pathlines flow visualization. This type of result can be used to predict where the stall begins, on which angle occurs at different lifting and control surfaces. This is extremely important due to the need to maintain a high level of safety during flight. What is more, changes to the aerodynamic layout of the aircraft also affect its stall characteristics.

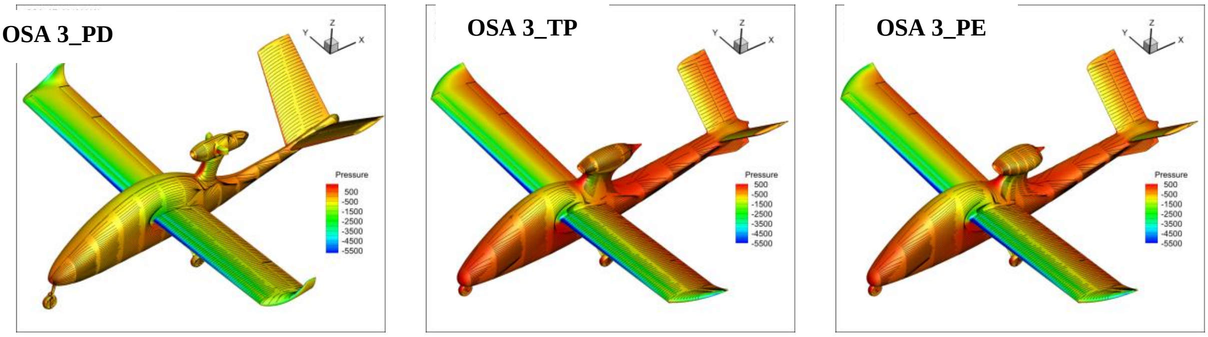

Figure 12 – Example of pressure distribution along with the pathlines flow visualization for three aircraft versions at the same angle of attack α=14°.

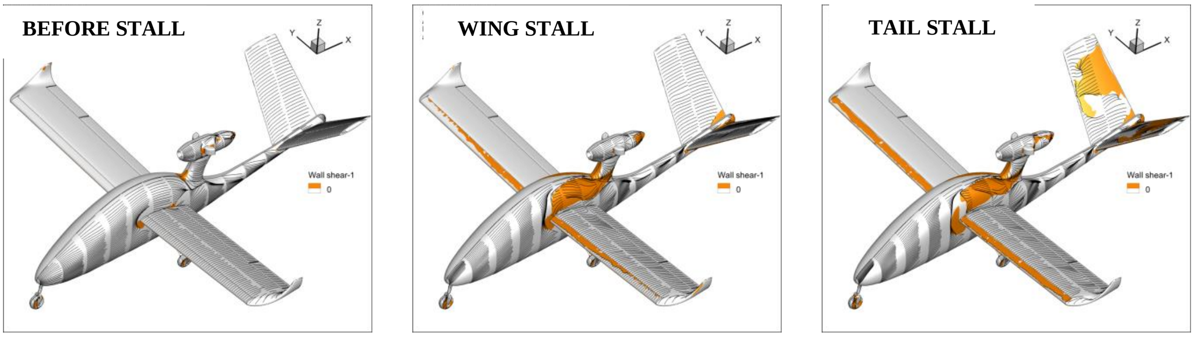

Figure 13 – Evolution of stall visualized by the areas of reverse flow (orange) along with the pathlines flow visualization: before stall (left), wing stall (middle) and the tail stall (right).

The results are also extended to compare the aerodynamic forces and moments for whole airframe and also its combination known as lift-to-drag ratio (Figure 14).

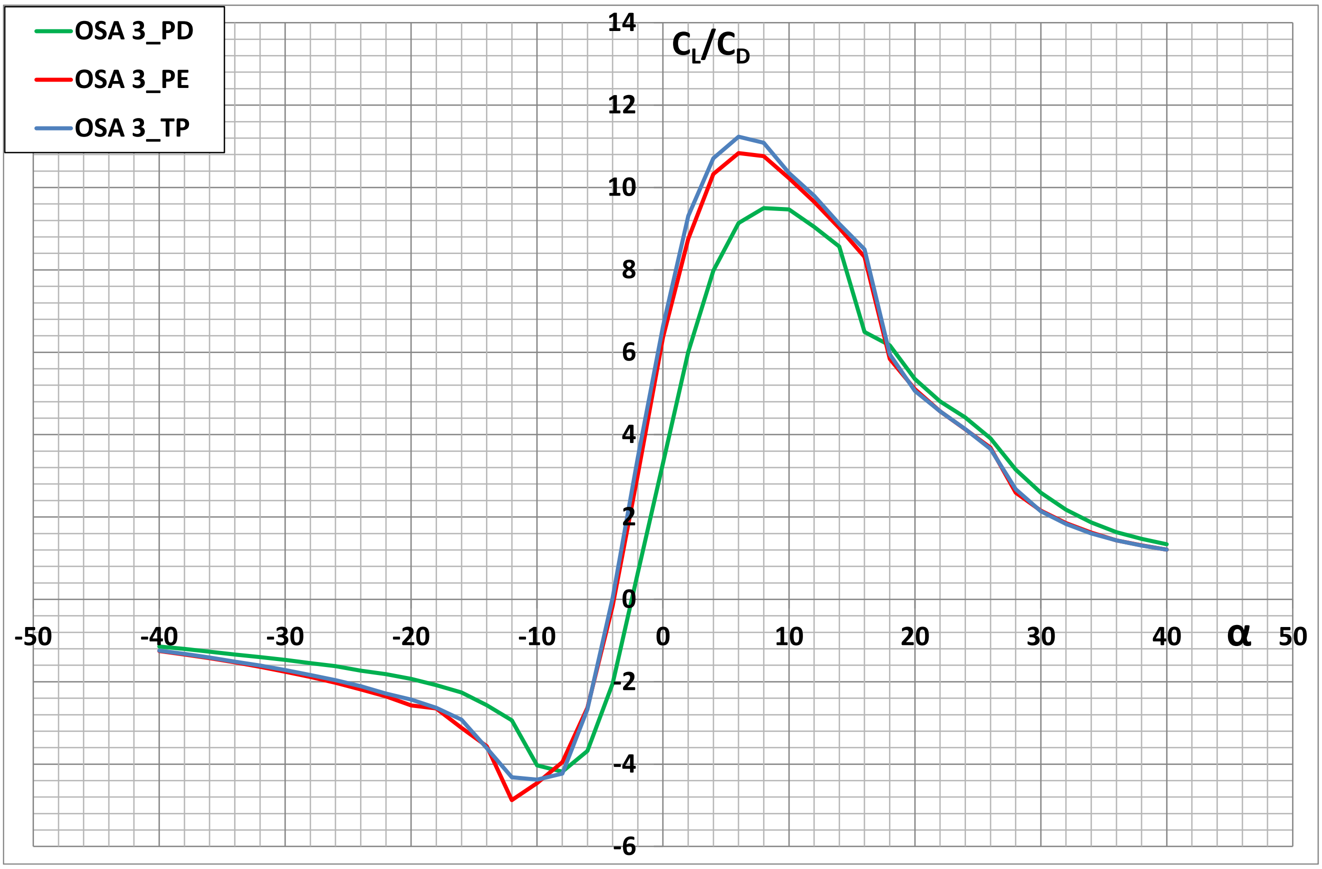

Figure 14 – The lift-to-drag ratio for three analysed configurations.

Already there, a clearly visible influence of fuselage change and also the nacelle change on improvement of the aerodynamic characteristics - are reasonably compared. The highest value of the lift-to-drag ratio was achieved for configuration OSA-3_TP (final aircraft version with turboprop engine) and it was 11.2. However, for configuration OSA-3_PD (initial aircraft version), the maximum value of this coefficient was only 9.5.

5. The Conclusion

In the course of the research work, a number of numerical aerodynamic analyses of the New Generation Light Combat Airplane were carried out. Numerical analyses were performed using the finite volume method, specialized software and a high-performance computing cluster. Both quantitative and qualitative results were obtained. The obtained results will have a significant impact on the decisions of the research team regarding the final shape of the airplane being developed. Therefore, the process of using the aerodynamic characteristics as the leading conclusion in changes of the design has been shown in this paper. The benefit of using these CFD tools in the design process earlier than at the end of this process, to see if some changes can be made or problems avoided early on, is no doubt already proven by more and more scientific work. The results shown here are yet another proof of validity of those methods, but also do show the improvement in context of the whole airframe properties, and how much that improvement is worth in comparison i.e. to change the size of the wingtip devices (winglets) on the lift and on the drag of airframe. Also, a negative drag of the slats being in overwhelming aerodynamic influence of wing is clearly visible which may be proof, that slats are working properly and it has an unbearable didactic value.

In addition, the resulting aerodynamic characteristics can be used during the stage of determining loads that act on the structure of the aircraft during the flight.

6. Contact Author Email Address

Corresponding author: lukasz.kiszkowiak@wat.edu.pl

7. Copyright Statement

References

[1] Torenbeek E., *Advanced Aircraft Design: Conceptual Design, Analysis and Optimization of Subsonic Civil Airplanes*, John Wiley & Sons, 2013.

[2] Walther, JN., Kocacan, B., Hesse, C. *et al.* Automatic cabin virtualization based on preliminary aircraft design data. *CEAS Aeronaut J* **13,** 403–418, https://doi.org/10.1007/s13272-021-00568-w, 2022.

[3] Raymer D., *Aircraft Design: A Conceptual Approach*, American Institute of Aeronautics and Astronautics, Inc. 2012.

[4] Di Pasquale D, Verma D, Pagliuca G. Blended wing body (BWB) planform multidisciplinary optimisation (MDO) for early stage aircraft design using model based engineering. In: *ICAS 2021*: *32nd Congress of the International Council of the Aeronautical Sciences*, 6-10 September 2021, Shanghai, China, 2021.

[5] Olejnik A., Kiszkowiak Ł., Dziubiński A. CFD simulation of engine nacelle cooling on pusher configuration aircraft; *Aircraft Engineering and Aerospace Technology*; ISSN: 0002-2667; 2021; DOI: 10.1108/AEAT-12-2020-0290.

[6] *ANSYS. Fluent Theory Guide*, version 15.0; Ansys Inc.: Canonsburg, PA, USA, 2013.

[7] Anderson JD Jr. *Computational fluid dynamics – the basis with applications*. New York, NY: McGraw-Hill, 1995.

[8] Hirsch Ch. *Numerical Computation of Internal and External Flows: The Fundamentals of Computational Fluid Dynamics*, 2nd Edition, Butterworth-Heinemann, ISBN: 9780750665940. 2007.

[9] Olejnik A., Kiszkowiak Ł., Dziubiński A. Aerodynamic modeling process using Reverse Engineering and Computational Fluid Dynamics; *Earth and Space 2018: Engineering for Extreme Environments*; American Society of Civil Engineers; 2018; 12 pages; ISBN: 9780784481899; https://doi.org/10.1061/9780784481899.089; 2018.

[10] Halila G.L.O., Antunes A. P., Ricardo Galdino da Silva, João Luiz F. Azevedo Effects of boundary layer transition on the aerodynamic analysis of high-lift systems, *Aerospace Science and Technology*, Volume 90, 2019, Pages 233-245, ISSN 1270-9638, https://doi.org/10.1016/j.ast.2019.04.051.

[11] Goetzendorf-Grabowski T, Tarnowski A, Figat M, Mieloszyk J, Hernik B. Lightweight unmanned aerial vehicle for emergency medical service – Synthesis of the layout. *Proceedings of the Institution of Mechanical Engineers, Part G: Journal of Aerospace Engineering*. 235(1):5-21. doi:10.1177/0954410020910584, 2021.

[12] Klimczyk WA, Goraj Z. Analysis and optimization of morphing wing aerodynamics, *Aircraft Engineering and Aerospace Technology*, DOI:10.1108/AEAT-12-2017-0289;91: 538–546, 2019.

[13] A. Viviani, A. Aprovitola, G. Pezzella, C. Rainone, CFD design capabilities for next generation high-speed aircraft, *Acta Astronaut*, 2020.

[14] Olejnik A., Kiszkowiak Ł., Dziubiński A., Majcher M. Cooling improvement of an aircraft engine in pusher configuration, *2021 IEEE 8th International Workshop on Metrology for AeroSpace (MetroAeroSpace),* ISBN 978-1-7281-7557-7; pp. 58-62, DOI: 10.1109/MetroAeroSpace51421.2021.9511781, 2021.

[15] Rodzewicz M., Goraj Z., Tomaszewski A. Design and testing of three tailless unmanned aerial vehicle configurations built for surveillance in Antarctic environment, *Proceedings of the Institution of Mechanical Engineers Part G-Journal of Aerospace Engineering*, DOI:10.1177/0954410018797855, 2018.

[16] Alaa A. Osman, Amgad M Bayoumy Aly, E.E. Khalil, Osama Abdellatif Numerical Analysis of an External Store Separation From an Airplane;10.2514/6.2016-2143, 2016.

[17] Olejnik A., Dziubinski A., Kiszkowiak Ł., Separation safety analysis using CFD simulation and remeshing; *Aerospace Science and Technology*; Volume 106, 2020, 106190; ISSN 1270-9638; https://doi.org/10.1016/j.ast.2020.106190, 2020.

[18] Olejnik A., Dziubinski A., Kiszkowiak Ł.CFD simulation of empty fuel tanks separation from a trainer jet; *Aircraft Engineering and Aerospace Technology*; ISSN: 0002-2667; DOI: 10.1108/AEAT-12-2019-0247, 2020.

[19] Torenbeek E., Synthesis of Subsonic Airplane Design: An Introduction To the Preliminary Design of Subsonic General Aviation and Transport Aircraft, with Emphasis on Layout, Aerodynamic Design, Propulsion and Performance, Springer Science & Business Media, 2013.

[20] Kiszkowiak, Ł. *Analysis of airplane static and dynamic stability using scaled models*, PhD thesis, Military University of Technology, Warsaw (in polish), 2020.

[21] Bridel G., Goraj Z., Kiszkowiak Ł., Brevot J., Devaux J., Szczepański C., Vrchota P. Air combat training – high energy at lowest cost; *Aircraft Engineering and Aerospace Technology*; ISSN: 0002-2667; 2021; DOI: 10.1108/AEAT-12-2020-0296.

[22] *ANSYS ICEM CFD Tutorial Manual*, Ansys ICEM CFD 15, November, Canonsburg, PA, USA, 2013.